COMPUTATIONAL ANALYSES OF SUPERSONIC FLOWS OVER A DELTA WING AT HIGH ANGLES OF ATTACK

Genta IMAI*, Kozo FUJII, Akira OYAMA****
***Department of Aeronautics and Astronautics, University of Tokyo**
****Japan Aerospace Exploration Agency**

Keywords: *delta wing, supersonic flow, CFD, aerodynamic characteristics, high angle of attack*

Abstract

Supersonic flows over a 65-degrees sweep delta wing with a sharp leading edge at high angles of attack are computationally studied. Computational simulations with various free-stream Mach numbers show that there is a sudden change in flow fields between the free-stream Mach number of 0.8 and 1.2. Visualized images of the simulation results at different flow conditions show that this nonlinear behavior occurs as expansion waves from the leading edge accelerate the flow and shift the share layer closer to the surface when the Mach number at the leading edge becomes supersonic. The results also show that aerodynamic characteristics have a different trend below and above the free-stream Mach number of 1.0. The sudden change occurs not at the boundary of the classification proposed by the former studies. When the free-stream Mach number becomes supersonic, components of the three-dimensional flow structure such as primary vortex, vortex breakdown and windward flow have different nature, which lead to the nonlinear behavior of aerodynamic characteristics.

1 Introduction

Many of supersonic aircrafts use delta wings. Airplanes and space planes with the delta wing often fly at high angles of attack. In landing or taking off phase, they need to fly at very high angles of attack due to their poor aerodynamic performance at low speeds. In addition, future space plane may fly at high angle of attack even at transonic and supersonic speeds in the reentry phase.

It is well known that there appear two large counter-rotating leading edge vortices when flying at high angles of attack in low speeds. When flying much higher speeds, flow becomes complicated because there appear shock waves which interact with vortices.

The earliest attempt to understand supersonic flows around delta wings at various flow conditions for various wing geometries appeared in the work of Stanbrook and Squire [1]. By examining all the experimental data available, Stanbrook and Squire proposed the classification of the flow patterns based on the component of angle of attack normal to the leading edge α_N and the component of Mach number normal to the leading edge M_N (Fig. 1). They classified the flows into two types; attached flow and separated flow at the leading edge. The boundary line between these two types exists near M_N =1.0, and has come to be known as the Stanbrook-Squire boundary (Fig. 2). Miller and Wood [2] experimentally studied flows over delta wings with different leading edge sweep angles using oil flow, tufts, and vapor screen methods. They classified the flows into six patterns according to α_N and M_N, namely (I) Classical vortex, (II) Vortex with shock, (III) Separation bubble with shock, (IV) Shock-induced separation, (V) Shock with no separation and (VI) Separation bubble with no shock (Fig. 2). Szodruch and Peake [3] suggested a similar classification for much thicker wings than those used by Miller and Wood. Seshadri and Narayan [4] and Brodetsky

[5] proposed similar classifications by examining flow fields in more detail. However, there may exist other parameters to govern the flow fields. In addition, aerodynamic characteristics behind the flow classification have not been discussed.

Flow fields over a delta wing at various angles of attack and various Mach numbers from subsonic to supersonic flow are computationally simulated and the results are analyzed. The objective of the present study is to reveal the flow field mechanism behind the classification for the better understanding of the aerodynamic characteristics. The analysis focuses on the location of the primary vortex and the normal force coefficient with increasing the free-stream Mach number at a fixed angle of attack of 20 degrees; representative of the cases at high angles of attack.

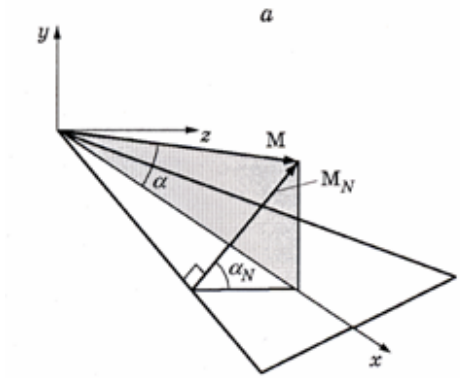

Fig. 1 Definition of α_N and M_N.

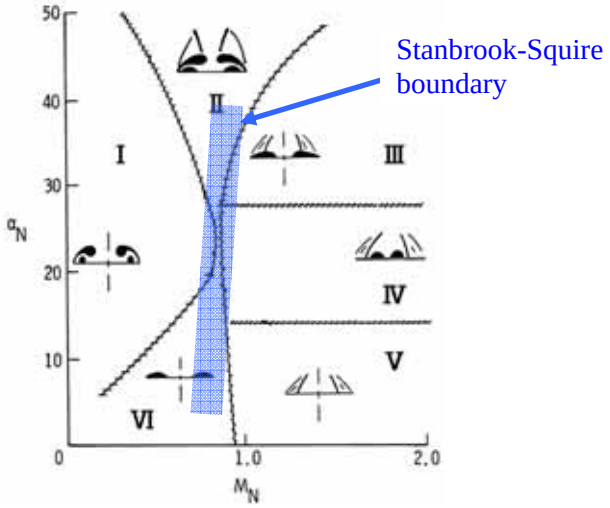

Fig. 2 Flow Fields classification chart by Miller and Wood [2].

2 Approaches

2.1 Numerical Methods

The governing equations are the three dimensional compressible (Favre-averaged) Navier-Stokes equations. Length, density and velocities are normalized by the length of root chord, the density and the speed of sound of the free-stream, respectively. Numerical fluxes for the convective terms are evaluated by the AUSM-DV [6] scheme extended to high-order space accuracy by the 3rd order upwind biased MUSCL interpolation [7] based on the primitive variables. The viscous terms are evaluated by the 2nd order central differencing. The LU-ADI factorized implicit algorithm [8] is used for the time integration. The flow fields are considered to be fully turbulent, and Baldwin-Lomax's algebraic turbulence model [9] with Degani-Schiff's modification is applied.

2.2 Model Geometry and Grid

The model geometry is shown in Fig. 3. The delta wing analyzed here has leading-edge sweep angle of 65 degrees. The leading edge is sharp and lee-surface is flat to reduce the effect of leading-edge shape on flow fields. Wing thickness ratio is 0.02 based on each chord length.

The flow fields are assumed to be symmetric on center line of the wing. Therefore, the computational domain covers only half of the wing. The computational grid (Fig. 4) is H-O topology with grid size of 2.16 million (153(chordwise) x 143(spanwise) x 99(normal)).

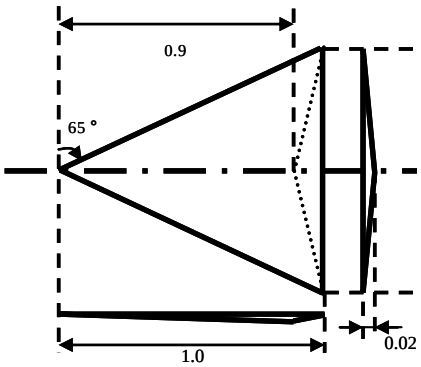

Fig. 3 Model geometry.

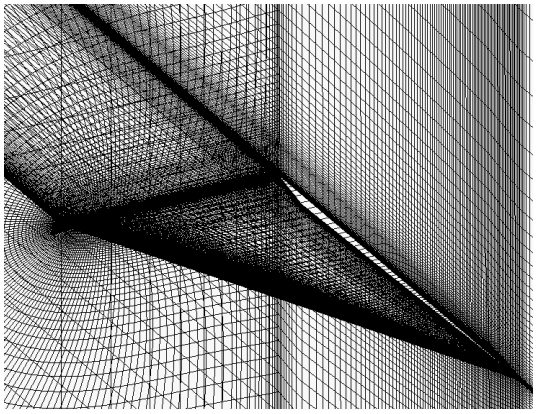

Fig. 4 Computational grid.

2.3 Flow Conditions

The flow conditions are chosen to cover the classification chart of Miller and Wood [2]. Free-stream Mach number M_∞ covers from 0.4 to 3.2 (incrementation by 0.4), angles of attack from 4 to 24 degrees (incrementation 4 degrees). Figure 5 shows the flow conditions plotted over the classification chart of Miller and Wood [2]. The selected Reynolds number based on the wing root-chord length is 1.3×10^6 according to the experiment of Miller and Wood [2].

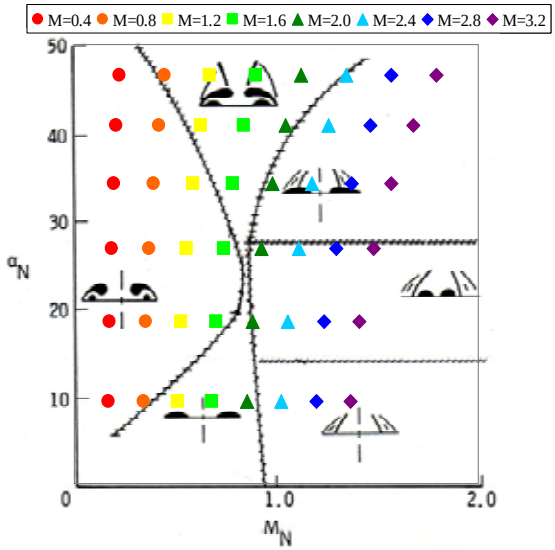

Fig. 5 Flow conditions of the present calculations.

2.4 Data Processing

Local time stepping method is used in the beginning of computations to converge steady solution earlier. After the solutions converge to certain extent, physical time stepping method is used in the computations. All of the flow fields and the aerodynamic coefficients in the following discussions are based on the time-averaged physical variables.

3 Results and Discussions

3.1 Flow Fields

3.1.1 Flow Field Classification

In Fig. 6, computational results are classified according to the vortex structure in the crossflow plane at 30% chordwise location. Flows with or without any shock waves are denoted by open or closed symbols, respectively. The circular symbols denote that primary and secondary vortices appear in the flow fields. The square symbols denote that the flows are dominated by separation bubbles. This figure shows that the present results are classified into almost the same types as those in the experimental results of Miller and Wood [2]. Note that the classification changes according to chordwise location as there occur vortex breakdown in some cases.

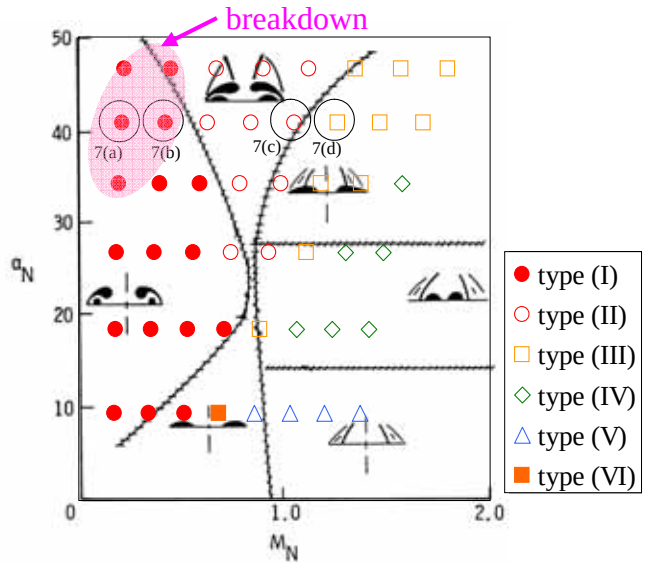

Fig. 6 Flow classification of the present calculation results.

3.1.2 Free-stream Mach Number Effect on Flow Field Transition

Figures. 7(a)-(d) show local Mach number contour map and total pressure contour lines in the crossflow plane at 30% chordwise station, the angle of attack of 20 degrees, and different free-stream Mach numbers (shown in Fig. 6).

The flow field at $M_\infty = 0.4$ (Fig. 7(a)) is classified into "classical vortex (type (I))" characterized by the primary and secondary vortices with no shock waves. While the flow field at $M_\infty = 0.8$ (Fig. 7(b)) can also be classified into "classical vortex (type (I)), a crossflow shock wave is observed between the primary vortex and the wing surface due to the flow acceleration under the primary vortex. Adverse pressure gradient due to this shock wave enhances the secondary flow separation. The flow field like this was indicated by the former studies [4, 5].

The flow field at $M_\infty = 2.0$ (Fig. 7(c)) is classified into "vortex with shock (type (II))". The spanwise flow acceleration induced by the primary vortex leads to the appearance of the shock wave over the primary vortex. This shock decelerates flow toward the wing root and changes the flow direction. The flow field at $M_\infty = 2.8$ (Fig. 7(d)) is classified into "separation bubble with shock (type (III))". Separation bubble is defined here as a vortex without secondary separation in the same manner described by Miller and Wood. This flow field is very similar to the flow field at $M_\infty = 2.0$, but secondary separation is not observed.

With increasing free-stream Mach numbers at constant angle of attack of 20 degrees, the flow field shifts from "classical vortex" to "vortex with shock" and "separation bubble with shock". Although the classification of the flow types depends on the definition, essence of the flow field transition is that the primary vortex becomes closer to the wing upper surface and gradually expands as the Mach number increases. Discussion in the next section focuses on the transition of the locations of the primary vortex cores.

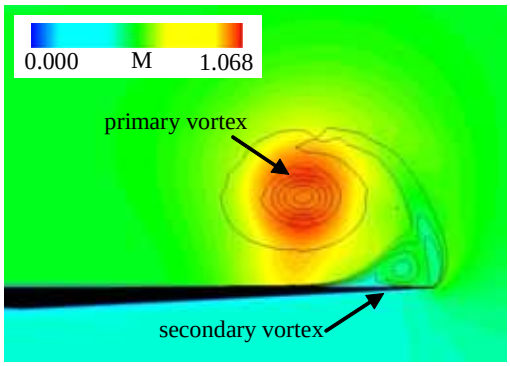

(a) $M_\infty = 0.4$ ($M_N = 0.21$)

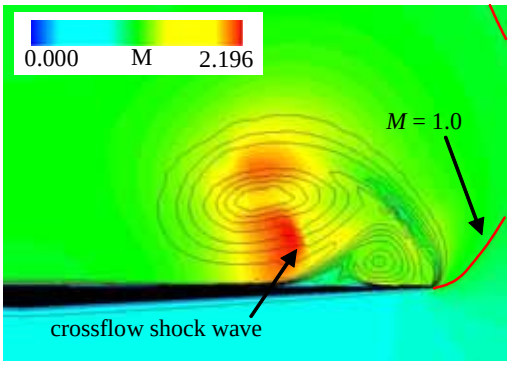

(b) $M_\infty = 0.8$ ($M_N = 0.42$)

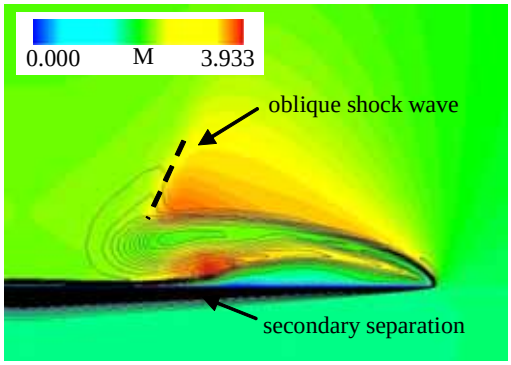

(c) $M_\infty = 2.0$ ($M_N = 1.12$)

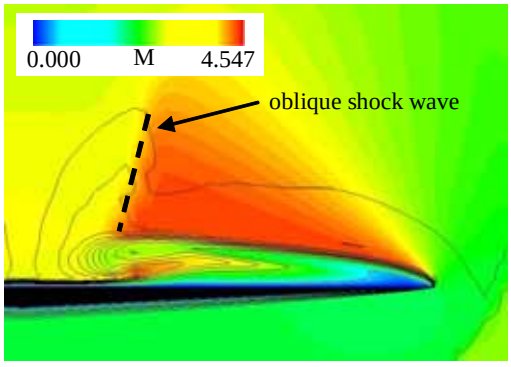

(d) $M_\infty = 2.8$ ($M_N = 1.57$)

Figs. 7 local Mach number contour map and total pressure contour lines in the crossflow plane at 30% chordwise station at α = 20 degrees – free-stream Mach number effect.

3.1.3 Locations of the Primary Vortex Core

Figure 8 shows how the spanwise positions of the primary vortex and its normal distances from the wing surface moves with the increases of the free-stream Mach numbers. They are measured at 30% chordwise station. Six cases at different angles of attack are presented. This figure shows that the vortex core moves toward inboard and lower as the free-stream Mach number increases. An interesting point is that under subsonic free-streams (M_∞=0.4 and 0.8) the normal distance from the wall stays almost same but under supersonic free-stream conditions (M_∞=0.8, 1.2, 1.6, 2.0 and 2.4) it significantly decreases.

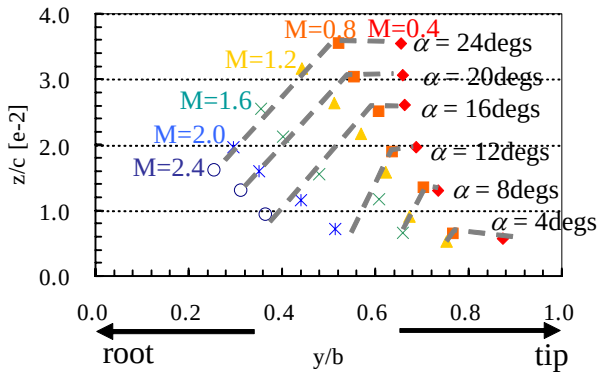

Fig. 8 Locations of the primary vortex cores.

Figure 9 shows vorticity contours near the leading edge at 30% chordwise station and different free-stream Mach numbers. This figure shows that the angle of the share layer to the wing surface stays almost the same under subsonic free-stream conditions (M_∞=0.4 and 0.8), but it becomes smaller and smaller as the Mach number still increases. This nonlinear move of the share layer with increasing Mach number causes the nonlinear move of the locations of the primary vortex core in Fig. 8.

Figure 10 shows the local Mach numbers at the point A indicated in Fig. 9. This figure shows that the flows turning around the leading edge become supersonic when M_∞=1.2 and 1.6.

Once the flow around the leading edge becomes supersonic, the expansion wave from the leading edge accelerates the flow and moves the share layer closer to the surface.

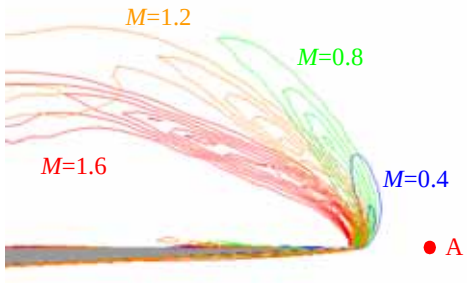

Fig. 9 Share layer near the leading edge at α = 20 deg.

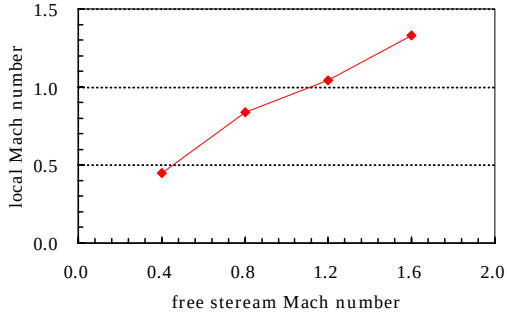

Fig. 10 Local Mach number at Point A.

3.2 Aerodynamic Characteristics

3.2.1 Mach Number Effect on the Normal Force Coefficients

Figure 11 shows the contours of normal force coefficient C_N plotted over the classification chart of Miller and Wood. Here, C_N and local pressure coefficient C_p are defined as

$$C_N = \iint_{surface} C_p \, dS$$

$$C_p = \frac{p - p_\infty}{\frac{1}{2}\rho_\infty U_\infty^2} = \frac{p - p_\infty}{\frac{1}{2}\gamma p_\infty M_\infty^2}$$

This figure shows C_N nonlinearly changes between M_∞ =0.8 and 1.2. In the flow conditions $M_\infty \le 1.2$, C_N increases as Mach number increases, but C_N decreases for the free-

stream conditions $M_\infty \geq 1.2$. Although not shown here, other aerodynamic coefficients (lift force coefficient C_L, drag force coefficient C_D and pitching moment coefficient C_M) also show similar behavior at M_∞ =1.2. This nonlinear behavior does not occur at the boundary of main flow types found in the former studies.

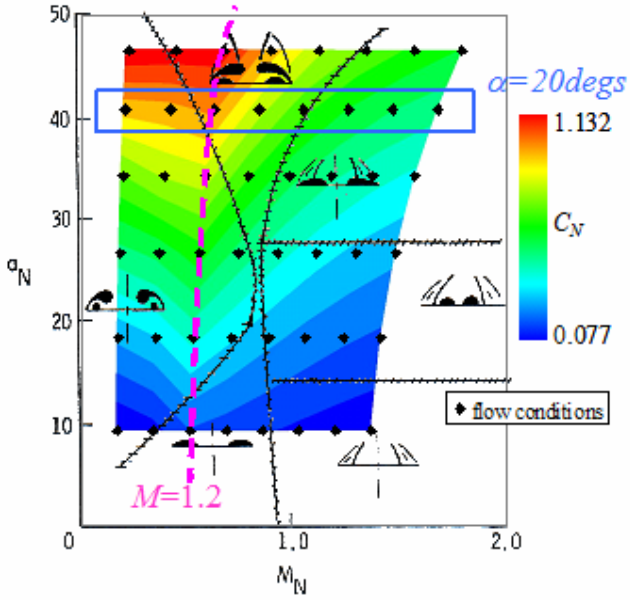

Fig. 11 C_N contours plotted over the classification chart of Miller and Wood.

Figure 12 shows C_N vs. free-stream Mach number. The upper and lower components of C_N (C_{Nu} and C_{Nl}) Both C_{Nu} and C_{Nl} changes nonlinearly at M_∞ =0.8 with increasing Mach numbers. As the Mach number increases, C_{Nu} is almost constant in the subsonic flow conditions (M_∞ = 0.4 and 0.8), but C_{Nu} decreases in the supersonic free- stream condition (M_∞ = 0.8, 1.2, 1.6, 2.0, 2.4, 2.8 and 3.2). On the other hand, C_{Nl} is almost constant at any Mach numbers except sudden jump between M_∞ = 0.8 and 1.2. The figure also shows C_N mainly depends on the lower-surface pressure in the supersonic flow conditions, while C_N mainly depends on the upper-surface pressure in the subsonic flow conditions.

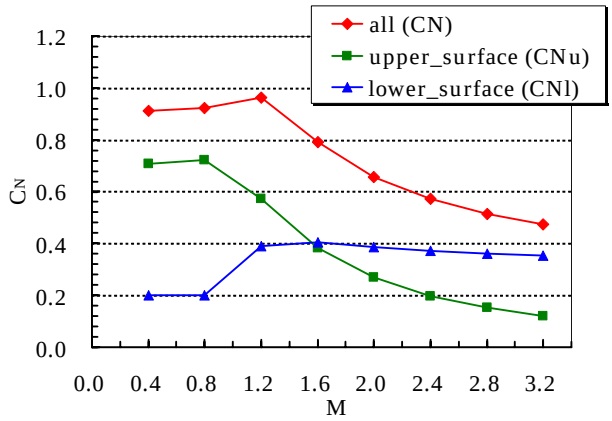

Fig. 12 Components of C_N on upper and lower surfaces at α = 20 degrees.

3.2.2 Contribution of Primary Vortex

Normal forces of the delta wing at low speeds mainly come from the contribution of the suction pressure created by the primary vortex. Thus it is important to estimate suction pressure. Figure 13 shows the Mach number effect on the pressure coefficient C_p at the primary vortex cores and the minimum C_p on the upper surface induced by the primary vortex. This figure shows that the minimum C_p on the surface increases with the C_p at the primary vortex core, which leads to decreases in the normal force. Focusing on C_{Nu} (shown in Fig. 12), C_{Nu} is almost constant in the subsonic flow conditions, although minimum C_p on the surface increases. So another elements dominant to normal force is discussed in the next section.

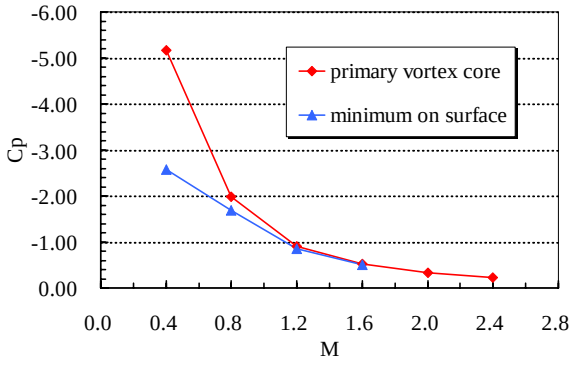

Fig. 13 Pressure coefficient at the primary vortex core at 30% chordwise station at α = 20 degrees.

3.2.3 Contribution of Vortex Breakdown to Normal Force

Upper sides of Figs. 14(a)-(c) show C_p contour plots in the wing symmetry plane and total pressure iso-surface in the plane of primary vortex. Lower side shows the C_p contour plots over the upper surfaces. At M_∞ = 0.4 and 0.8 (Fig.14(a) and (b)) the vortex breakdown occurs at 68% and 77% chordwise location, respectively. Increase of the free-stream Mach number moves the location of breakdown downstream. At higher Mach numbers, vortex breakdown dose not occur.

Upper surface C_p distributions at the wing root chord in Fig. 15 show the adverse pressure gradient disappears as the Mach number increases. That occurs due to the strong expansion wave from the wing apex (Fig. 14(c)). In the subsonic flow conditions, increase of Mach numbers make adverse pressure gradient in the chordwise direction smaller and smaller and the location of breakdown moves downstream, which leads to increases in the normal force. In the supersonic flow conditions, adverse pressure gradient disappears and breakdown does not appear which has an effect of making the normal force constant.

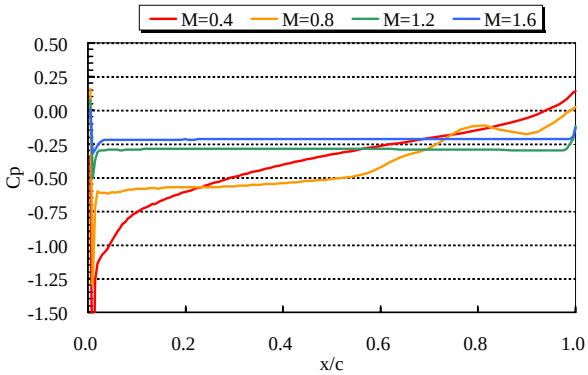

Fig. 15 Chordwise C_p distribution at the wing root at α = 20 degrees.

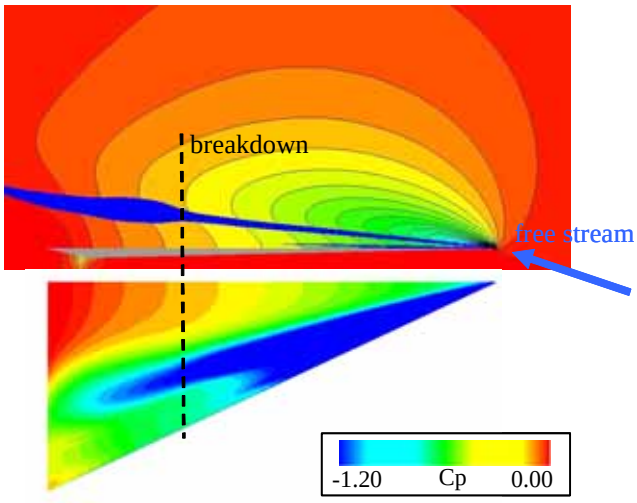

(a) M_∞ = 0.4 (M_N = 0.21)

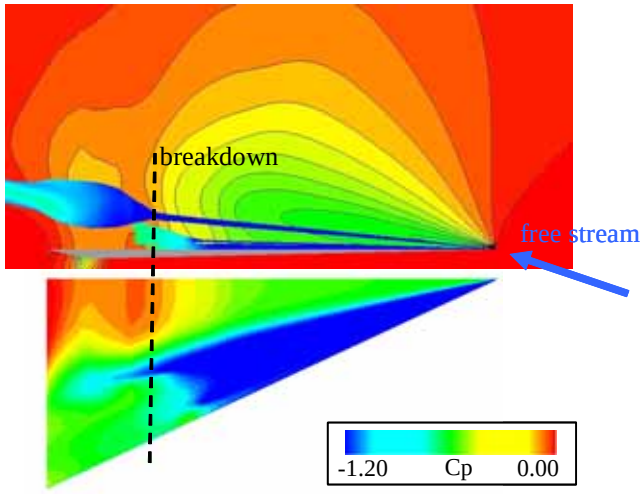

(b) M_∞ = 0.8 (M_N = 0.42)

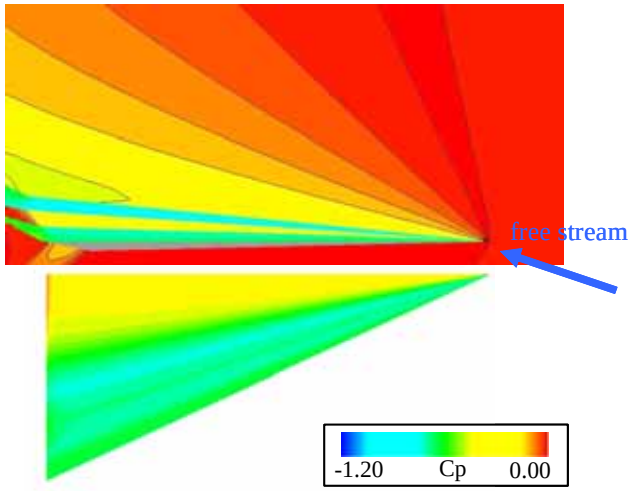

(c) M_∞ = 1.2 (M_N = 0.63)

Figs. 14 C_p distributions on the upper symmetry planes and the wing upper surfaces at α = 20 degrees.

3.2.4 Normal Force on the Lower Surface

The normal force component for the lower surface has a sudden change between $M_\infty = 0.8$ and 1.2(Fig. 12).

Figures 16 show C_p distributions in the wing lower symmetry plane of the flows at Mach numbers of 0.8 and 1.6. At $M_\infty = 1.6$ (Fig. 17(b)), the free stream becomes supersonic at the wing apex. There appear attached shock wave from the wing apex and expansion wave from the wing tailing edge. This shock wave decelerates the chordwise velocity and raises the pressure.

Figure 17 shows lower surface C_p distribution in the wing root section at different Mach numbers of 0.4, 0.8, 1.2 and 1.6. This figure indicates that an increase in Mach number raises the average level of C_p and the pressure gradient. The pressure gradient reaches to almost 0 in the supersonic flow conditions, because the windward flow is decelerated by the attached shock from the wing apex. These shifts of the flow fields caused C_N sudden jump between $M_\infty = 0.8$ and 1.2.

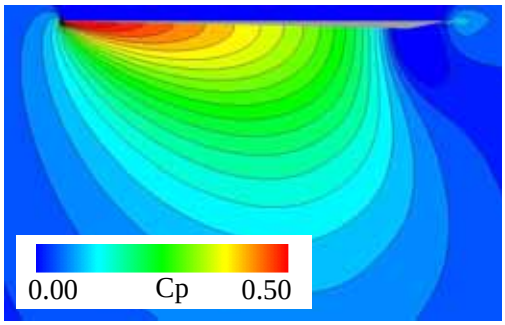

(a) $M_\infty = 0.8$ ($M_N = 0.42$)

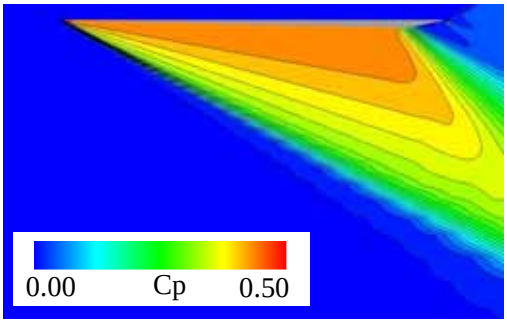

(b) $M_\infty = 1.6$ ($M_N = 0.84$)

Figs. 16 C_p distributions on the lower symmetry planes at $\alpha = 20$ degrees.

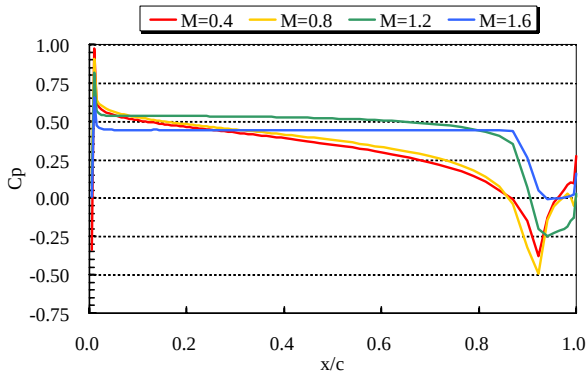

Fig. 17 Chordwise C_p distribution at the wing root at $\alpha = 20$ degrees.

3.2.4 Summary of the Flow Field behind the Normal Force Characteristics

Table 1 summarizes flow field effects on the characteristics of the normal force coefficient. Under the subsonic and transonic free-stream conditions, effects on C_N of each component in flow structures such as primary vortex, vortex breakdown and windward flow make C_N constant for increase of the free-stream Mach number. Under the supersonic free-stream conditions, vortex breakdown and windward flow is fixed; which has an effect of making C_N constant. The C_p at the primary vortex core increases; which leads to decrease in C_N. Therefore, total C_N is decreased in the supersonic free-stream condition.

Table 1 Summary of flow field effects on C_N characteristics with increasing free-stream Mach number.

		Subsonic	Transonic	Supersonic
		M = 0.4 -> 0.8	M = 0.8 -> 1.2	M = 1.2 -> 3.2
Primary Vortex	flow field	incresing C_p at the vortex core		
	C_N	decrease		
Vortex Breakdown	flow field	shifting to downsteam	not occurred	
	C_N	increase	constant	
Lower Surface Flow	flow field	without shock from the apex	with shock from the apex	
	C_N	constant	increase	constant
Total C_N		constant		decrease

4 Conclusions

In the present study, subsonic to supersonic flows over a delta wing at high angles of attack have been computationally investigated. The results show that the nonlinear behavior of the locations of the primary vortex core between free-stream Mach number of 0.8 and 1.2 with increasing the Mach number. This nonlinear behavior occurs as expansion wave from the leading edge accelerates the flow and shifts the share layer closer to the surface, when the flow turning around the leading edge becomes supersonic. The results also show that normal force coefficient has a different trend below and above the free-stream Mach number of 1.0. This change of normal force characteristics occurs not at the boundary of the classification of main flow types indicated by the former studies. When the free-stream Mach number becomes supersonic, the components of three-dimensional flow structure such as primary vortex, vortex breakdown and windward flow has a different nature, which lead to the nonlinear behavior of aerodynamic characteristics.

References

[1] Stanbrook A. and Squire L. C. Possible types of flow at swept leading edges. *Aeronautical Quarterly*, Vol.15, No. 2, pp 72-82, 1964.

[2] Miller D. S and Wood R. M. Leeside Flows over delta wings at supersonic speeds. *Journal of Aircraft*, Vol. 21, No. 9, pp 680-686, 1984.

[3] Szodruch J. G and Peake D. J. Leeward flow over delta wings at supersonic speeds. NASA-TM, No. 81187, 1980.

[4] Seshadri S. N and Narayan K. Y. Possible types of flow on lee-surface of delta wings at supersonic speeds. *Aeronautical Journal*, No. 5, 185-199, 1988.

[5] Brodetsky M. D, Krause E, Nikiforov S. B, Pavlov A. A, Kharitonov A. M, and Shevchenko A. M. Evolution of vortex structures on the leeward side of a delta wing. *Journal of Applied Mechanics and Technical Physics*, Vol. 42, No. 2, pp 242-254, 2001

[6] Wada Y. and Liou M. S. A flux splitting scheme with high-resolution and robustness for discontinuities. AIAA paper, 94-0083, 1994

[7] Van Leer B. Toward the ultimate conservative difference scheme. 4. *Journal of Computational Physics*, Vol. 23, pp 276-299, 1977.

[8] Fujii K. and Obayashi S, Practical applications of new LU-ADI scheme for the three-dimensional Navier-Stokes computation of transonic viscous flows. AIAA paper, 86-513, 1986.

[9] Baldwin B and Lomax H. Thin layer Approximation and algebraic model for separated turbulent flows. AIAA paper 78-257, 1978.